Amplitude suppression of oscillators with delay connections and slow switching topology

Amplitude suppression of oscillators with delay connections and slow switching topology

Tetsu Iwamoto,[1] Yoshiki Sugitani,[2] Shinnosuke Masamura,[1] Keiji Konishi,[1,*] and Naoyuki Hara[1]
[1]*Department of Electrical and Information Systems, Osaka Prefecture University, 1-1 Gakuen-cho, Naka-ku, Sakai, Osaka 599-8531, Japan*
[2]*Department of Electrical and Electronic Systems Engineering, Ibaraki University, 4–12–1 Nakanarusawa, Hitachi, Ibaraki 316-8511, Japan*

(Received 27 March 2020; accepted 12 August 2020; published 8 September 2020)

The present paper shows that the amplitudes of oscillators in delay-coupled oscillator networks can be suppressed by switching the network topology at a rate much lower than the oscillator frequencies. The mechanism of suppression was clarified numerically, and a procedure for determining the connection parameters to induce suppression is presented. The analytical and numerical results were obtained with Stuart–Landau oscillators and were experimentally validated using double-scroll chaotic circuits.

DOI: 10.1103/PhysRevE.102.032206

I. INTRODUCTION

Quenching phenomena in coupled oscillators, which are induced by mutual connections, have been recently intensively investigated in the field of nonlinear physics [1,2]. It is well known that these phenomena can be classified into the two types of quenching: oscillation death and amplitude death [2]. Oscillation death is an invasive emergence of stable equilibrium points in coupled oscillators; in this phenomenon, the coupling signals converge to a constant nonzero value when oscillation death occurs. In contrast, amplitude death is a noninvasive stabilization of equilibrium points embedded within isolated oscillators; when amplitude death occurs, all the coupling signals converge to zero. The noninvasiveness of the latter phenomenon, which allows the coupling signals through connections to be small, has the advantage of enabling the utilization of death to suppress undesired oscillations in engineering applications. For this reason, amplitude death has great potential for use in engineering systems, such as direct current (DC) bus systems [3] and thermoacoustic systems [4,5].

The types of connections that induce amplitude death are roughly categorized into no-delay and delay connections. The no-delay connection, the simplest diffusive connection, can induce amplitude death in nonidentical oscillators, but not in identical oscillators [6–8]. In contrast, the delay connection can induce amplitude death even in identical oscillators[1] and can enlarge the death region in the connection parameter space [9,10]. In addition, there remains an ever-increasing interest and challenge to accumulate knowledge on delay-connection-induced amplitude death [15–24], as the transmission delays of signals passing through connections cannot be ignored in real systems.

Most previous studies on delay-connection-induced amplitude death focused only on delay-coupled oscillator networks with topologies that are temporally *fixed*. It is necessary to consider delay-connection-induced amplitude death in time-varying oscillator networks because there are numerous networks whose topologies are temporally *variable* in practical situations. However, it is still a great challenge to analyze the stability of coupled oscillators with both delay connections and time-varying topologies. This type of system was evaluated in the case where the topology changed at a rate much higher than the oscillator frequency [25], which simplifies the stability analysis. In addition, this analytical approach was recently extended and verified using experimental circuits [26].

The purpose of this study was to deal with the *opposite* situation for delay-coupled oscillator networks: topologies change at a rate that is much *lower* than the oscillator frequency. It was observed that such slow-switching topologies can suppress the oscillator amplitude around an unstable equilibrium point embedded within isolated oscillators. The mechanism behind this amplitude suppression is shown to be the formation of two clusters of antiphase synchronized oscillators induced by the delay connection, where the slow-switching topology acts to counteract this cluster formation. This mechanism was verified numerically, and a procedure for inducing amplitude suppression was developed. The analytical and numerical results were obtained using Stuart–Landau oscillators. In addition, these results were experimentally validated using double-scroll chaotic circuits.

A preliminary version of the present paper was presented at an international symposium [27]. The present paper significantly extends the preliminary results as follows: the necessary conditions for amplitude suppression are clarified, the relationship between these conditions and the connection parameters is revealed, the procedure for determining these parameters to induce suppression is provided, and the influence of these parameters and the switching period on the suppression is investigated numerically and experimentally.

---

[*] http://www.eis.osakafu-u.ac.jp/∼ecs.

[1] It should be noted that amplitude death in identical oscillators can be induced by other connections, such as dynamic connections [11], conjugate connections [12], direct and indirect connections [13], and mean-field connections [14].

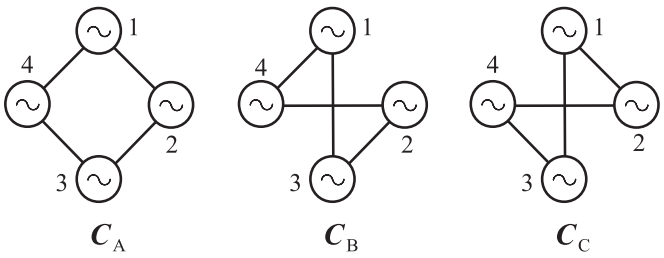

FIG. 1. Illustration of three topologies $\boldsymbol{C}_A$, $\boldsymbol{C}_B$, and $\boldsymbol{C}_C$.

II. SUPPRESSION OF THE AMPLITUDE OF DELAY-COUPLED OSCILLATORS

Let us consider four identical Stuart–Landau oscillators:

$$\dot{Z}_j(t) = \{1 + i\omega - |Z_j(t)|^2\}Z_j(t) + U_j(t), \tag{1}$$

where $Z_j(t) \in \mathbb{C}$ is the state variable of oscillator $j \in \{1, \ldots, 4\}$ at time $t \geqslant 0$, and $\omega \in \mathbb{R}$ is the common frequency of the four oscillators. The four oscillators described in Eq. (1) are coupled by the coupling signal

$$U_j(t) = \frac{k}{2}\sum_{l=1}^{4} c_{jl}(t)\{Z_l(t-\tau) - Z_j(t)\}, \tag{2}$$

where $k \geqslant 0$ and $\tau \geqslant 0$ are the coupling strength and delay time, respectively. Additionally, $c_{jl}(t)$ describes the topology of the coupled oscillators at time $t \geqslant 0$; if oscillator j is (is not) connected to oscillator l at time t, then $c_{jl}(t) = c_{lj}(t) = 1$ ($c_{jl}(t) = c_{lj}(t) = 0$). The elements of the adjacency matrix $\boldsymbol{C}(t)$ for the connections are represented as $c_{jl}(t) = \{\boldsymbol{C}(t)\}_{jl}$. It should be noted that the oscillator frequency in Eq. (1) is fixed at $\omega = 4\pi$ throughout this paper.

The present paper focuses on a *ring*-type network with oscillators described by Eq. (1) and connections described by Eq. (2) [30–33]. Let us consider the following three adjacency matrices (see Fig. 1):

$$\boldsymbol{C}_A := \begin{bmatrix} 0 & 1 & 0 & 1 \\ 1 & 0 & 1 & 0 \\ 0 & 1 & 0 & 1 \\ 1 & 0 & 1 & 0 \end{bmatrix}, \quad \boldsymbol{C}_B := \begin{bmatrix} 0 & 0 & 1 & 1 \\ 0 & 0 & 1 & 1 \\ 1 & 1 & 0 & 0 \\ 1 & 1 & 0 & 0 \end{bmatrix},$$

$$\boldsymbol{C}_C := \begin{bmatrix} 0 & 1 & 1 & 0 \\ 1 & 0 & 0 & 1 \\ 1 & 0 & 0 & 1 \\ 0 & 1 & 1 & 0 \end{bmatrix}.$$

It is clear that these topologies are *equivalent* to a ring topology; thus, phenomena that emerge with a time-*invariant* topology given by $\boldsymbol{C}(t) \equiv \boldsymbol{C}_A$, $\boldsymbol{C}_B$, or $\boldsymbol{C}_C$ are identical. However, this study deals with the time-*variant* network topology $\boldsymbol{C}(t) \in \{\boldsymbol{C}_A, \boldsymbol{C}_B, \boldsymbol{C}_C\}$ that switches between these three topologies.[2] The switching period T is presumed to be much longer than the natural period of the oscillators, i.e., $T \gg 2\pi/\omega$; this long period implies that the network topology slowly switches between the three defined topologies.

[2]Stabilization and synchronization of Stuart–Landau oscillators on fast time-variant networks have been recently reported [28,29].

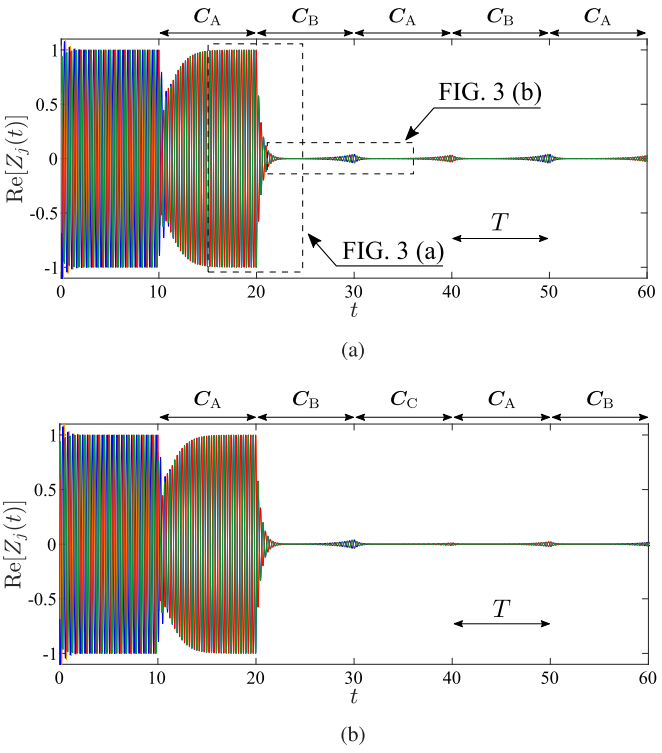

FIG. 2. Time series data for state variables $Z_j(t)$: (a) topology switching $\boldsymbol{C}_A \to \boldsymbol{C}_B \to \boldsymbol{C}_A \to \cdots$ and (b) topology switching $\boldsymbol{C}_A \to \boldsymbol{C}_B \to \boldsymbol{C}_C \to \cdots$ ($k = 3.00$, $\tau = 0.25$, $T = 10.0$).

Here we consider two examples of numerical simulations. First, the network topology is defined as $\boldsymbol{C}(t) \in \{\boldsymbol{C}_A, \boldsymbol{C}_B\}$ and switched between $\boldsymbol{C}_A$ and $\boldsymbol{C}_B$ with period T. Figure 2(a) shows time series data for the state variables $Z_j(t)$ in this simulation with connection parameters $(k,\ \tau) = (3.00,\ 0.25)$ and a switching period of $T = 10.0 \gg 2\pi/\omega = 0.5$. Note that the uniform random numbers $\xi_j(t) \in \mathbb{C}$ in the narrow range, $\mathrm{Re}[\xi_j(t)] \in [-0.01,\ 0.01]$ and $\mathrm{Im}[\xi_j(t)] \in [-0.01,\ 0.01]$, are added to the right-hand side of Eq. (1) and updated at time intervals of 0.1. The four oscillators were isolated until $t = 10$, at which point they were coupled with the network topology $\boldsymbol{C}(t) = \boldsymbol{C}_A$. The topology then switched to $\boldsymbol{C}(t) = \boldsymbol{C}_B$ at $t = 20$ and continued to alternate in this manner in time intervals of 10. It can be seen that the amplitudes of all the oscillators were suppressed just after the topology changed from $\boldsymbol{C}_A$ to $\boldsymbol{C}_B$. After a while, the amplitude gradually increased; however, it was suppressed when the next switch occurred.

In the second simulation, the network topology was defined as $\boldsymbol{C}(t) \in \{\boldsymbol{C}_A, \boldsymbol{C}_B, \boldsymbol{C}_C\}$ and switched among the three possible states in a given order. The time series data for $Z_j(t)$ in this simulation are shown in Fig. 2(b). As with the first simulation, the amplitudes of the oscillators were suppressed by switching between these three topologies.

The time series data for $t \in (10, 20]$ in Fig. 2 demonstrate that coupled oscillators with $\boldsymbol{C}(t) \equiv \boldsymbol{C}_A$ show oscillatory behavior and their amplitude is never suppressed. This indicates that coupled oscillators with $\boldsymbol{C}(t) \equiv \boldsymbol{C}_B$ or $\boldsymbol{C}_C$ would behave in the same way as those with $\boldsymbol{C}(t) \equiv \boldsymbol{C}_A$, as these three

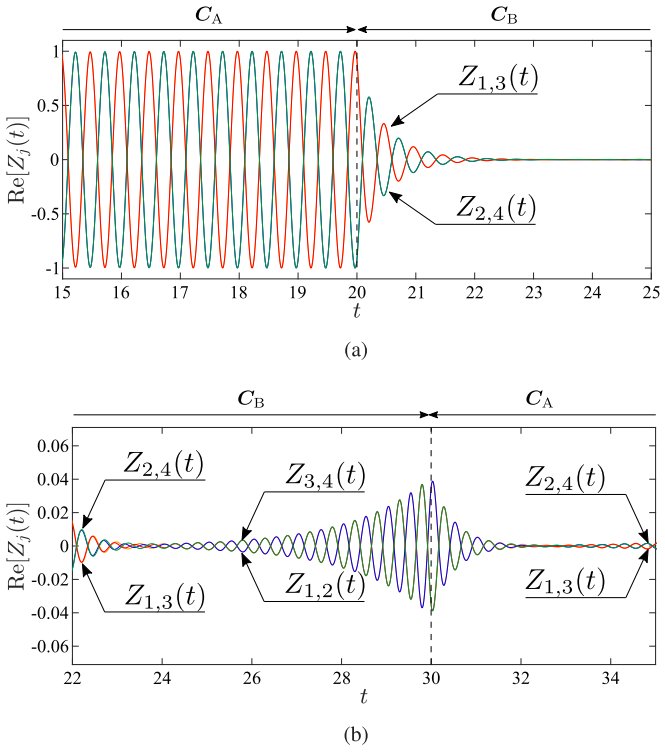

FIG. 3. Enlarged views of time-series data in Fig. 2(a) for (a) $t \in [15, 25]$ and (b) $t \in [22, 35]$.

topologies are equivalent. The two numerical examples described above demonstrate that a slow-switching topology can suppress oscillations.

III. MECHANISM AND DESIGN

This section describes the mechanism behind oscillation suppression and provides a simple procedure for determining (k, τ) to induce this suppression. In addition, we numerically investigate the influence of (k, τ) and the switching period T on the suppression.

A. Mechanism of suppression

To clarify the mechanism of suppression, the time series data for the oscillators were observed in more detail. Figure 3(a) shows an enlarged view of the time-series data presented in Fig. 2(a) for $t \in [15, 25]$. In the scenario represented in this plot, for $t \in [15, 20]$, oscillator 1 with $\boldsymbol{C}(t) = \boldsymbol{C}_A$, which is connected to oscillators 2 and 4, is synchronized in-phase with oscillator 3 but antiphase with oscillators 2 and 4:

$$Z_1(t) \approx -Z_2(t) \approx Z_3(t) \approx -Z_4(t). \tag{3}$$

After $\boldsymbol{C}(t)$ switched from $\boldsymbol{C}_A$ to $\boldsymbol{C}_B$ at time $t = 20$, oscillator 1 became connected to oscillators 3 and 4. Thus, the initial state of the oscillators for topology $\boldsymbol{C}_B$ at $t = 20$ is described by Eq. (3) for $t \in [20 - \tau, 20]$. Because Eq. (3) still holds until $t \approx 23$ even after switching, the coupling signals (2) after switching are then reduced to $U_j(t) \approx -kZ_j(t)$ $(j = 1, \ldots, 4)$. Accordingly, the coupled oscillators after switching are approximately given by

$$\dot{Z}_j(t) = \{(1 - k) + i\omega - |Z_j(t)|^2\}Z_j(t), (j = 1, \ldots, 4). \tag{4}$$

The equilibrium points of the oscillators described by Eq. (4), $Z_j(t) \equiv 0$, are stable (unstable) for $1 - k < 0$ $(1 - k > 0)$; these points with the parameter $k = 3.00$ used in Figs. 2(a) and 3 are therefore stable. Thus, for $t \in [20, 23)$, the oscillations for all of the oscillators decrease in amplitude.

Figure 3(b) shows an enlarged view of the time-series data for $t \in [22, 35]$. It can be seen that after the decrease in amplitude, the states of the oscillators for $t \in [23, 24)$ stray from the antiphase synchronization described by Eq. (3) because of the presence of a small amount of noise $\xi_j(t) \in \mathbb{C}$ added to the right-hand side of Eq. (1). For $t \in [24, 30)$, the amplitude of the oscillators then increases with another antiphase synchronization, described by

$$Z_1(t) \approx Z_2(t) \approx -Z_3(t) \approx -Z_4(t). \tag{5}$$

In other words, at approximately $t \in [23, 24]$, the small amount of added noise $\xi_j(t)$ causes the oscillators to switch from the antiphase synchronization state described by Eq. (3), which stably occurs with topology $\boldsymbol{C}_A$, to a second antiphase synchronization state described by Eq. (5), which stably occurs with topology $\boldsymbol{C}_B$. It should be noted that if noise is not added to the oscillators, the state requires a very long time to stray from the first antiphase synchronization state [Eq. (3)] in a numerical simulation. This suggests that the noise is a necessary factor to achieve the switching of synchronizations with the finite switching period T. The same behavior was also observed for $t \in [28, 35]$. It can thus be concluded that the essential mechanism for the slow-switching-topology-induced suppression in Fig. 2 is the repetition of the following actions in order: antiphase synchronization, switching of the topology, amplitude decrease, switching to another antiphase synchronization state, and slow amplitude increase with this second antiphase synchronization state.

The above discussion indicates that the following three conditions are necessary for amplitude suppression: (i) $k > 1$ holds for the stability of the equilibrium points in the oscillators [Eq. (4)]; (ii) an antiphase synchronization state exists, but other synchronizations, including in-phase synchronization and splay states, do not exist; (iii) the existing antiphase synchronization state is stable. Therefore, if one wants to induce the suppression of the oscillations, k and τ should be chosen such that the above three conditions are satisfied.

B. Design of connection

The connection parameters k and τ were then chosen such that the above three conditions hold. Because condition (i) is easily implemented, conditions (ii) and (iii) are discussed below. It should be noted that as the three considered topologies $\boldsymbol{C}_A$, $\boldsymbol{C}_B$, and $\boldsymbol{C}_C$ are equivalent, it is possible to consider only $\boldsymbol{C}_A$ without a loss of generality.

The dynamics of delay-coupled oscillator networks described by Eqs. (1) and (2) with $\boldsymbol{C}_A$ can be described in polar

form as

$$\dot{r}_j(t) = h(r_j(t)) + \frac{k}{2} r_{j-1}(t-\tau)\cos\left(\theta_{j-1}(t-\tau) - \theta_j(t)\right) + \frac{k}{2} r_{j+1}(t-\tau)\cos\left(\theta_{j+1}(t-\tau) - \theta_j(t)\right), \quad (6)$$

$$\dot{\theta}_j(t) = \omega + \frac{k}{2}\frac{r_{j-1}(t-\tau)}{r_j(t)}\sin\left(\theta_{j-1}(t-\tau) - \theta_j(t)\right) + \frac{k}{2}\frac{r_{j+1}(t-\tau)}{r_j(t)}\sin\left(\theta_{j+1}(t-\tau) - \theta_j(t)\right), \quad (7)$$

where

$$r_j(t)e^{i\theta_j(t)} := Z_j(t), \ \ h(r) := (1-k-r^2)r.$$

A ring network with periodic boundary conditions was implemented by setting $Z_0(t) = Z_4(t)$ and $Z_5(t) = Z_1(t)$.

First, condition (ii) is addressed. In phase-synchronized states, each oscillator has a constant phase difference of $m\pi/2$ with respect to the remaining connected oscillators, and the oscillators have a common amplitude $\hat{r} > 0$ and frequency $\Omega > 0$. Such states can be described by

$$r_j(t) = \hat{r}, \quad \theta_j(t) = \hat{\theta}_j^{(m)}(t) := \Omega t + (j-1)\frac{m}{2}\pi, \quad (8)$$

where $m \in \{0, 1, 2, 3\}$ describes the type of synchronization: in-phase ($m = 0$), antiphase ($m = 2$), and splay ($m = 1$ or 3). Substituting Eq. (8) into the polar-form state equation given in Eqs. (6) and (7) yields

$$\hat{r}^2 = 1 - k\left(1 - \cos\Omega\tau\cos\frac{m}{2}\pi\right) > 0, \quad (9a)$$

$$\Omega = \omega - k\sin\Omega\tau\cos\frac{m}{2}\pi. \quad (9b)$$

Note that there exists synchronization as described by Eq. (8) with type m if Eqs. (9a) and (9b) hold. Thus, the antiphase synchronization with a common frequency of Ω satisfying Eq. (9b) with $m = 2$ exists if k and τ satisfy

$$\hat{r}^2 > 0 \Leftrightarrow 1 - k(1 + \cos\Omega\tau) > 0. \quad (10)$$

In contrast, the in-phase synchronization with Ω satisfying Eq. (9b) with $m = 0$ does *not* exist if k and τ satisfy

$$\hat{r}^2 < 0 \Leftrightarrow 1 - k(1 - \cos\Omega\tau) < 0. \quad (11)$$

Furthermore, for $k > 1$ [condition (i)], synchronization with $m = 1$ or 3 (i.e., splay states) never exists, independent of k and τ. This is because Eq. (9a) cannot yield a real positive $\hat{r}^2$ with $k > 1$ [condition (i)] for $m = 1$ or 3. This suggests that the coexistence of a splay state does not need to be considered. The above discussion demonstrates that if k and τ satisfy both Eqs. (10) and (11), then condition (ii) is satisfied.

The regions satisfying condition (ii) in (k, τ) parameter space are now described (see Fig. 4). The red (blue) curves in the figure are values of (k, τ) that satisfy $\hat{r}^2 = 0$ with $m = 2$ ($m = 0$). The amplitude $\hat{r}$ grows from zero with increasing (decreasing) τ on the bold (thin) curves.[3] Additionally, there exists antiphase (in-phase) synchronization outside the regions between the bold and thin red (blue) curves. Thus, in the blue (red) regions, antiphase (in-phase) synchronization exists and does not coexist with in-phase (antiphase) synchronization, and (k, τ) values satisfying condition (ii) are the blue regions in the parameter space.

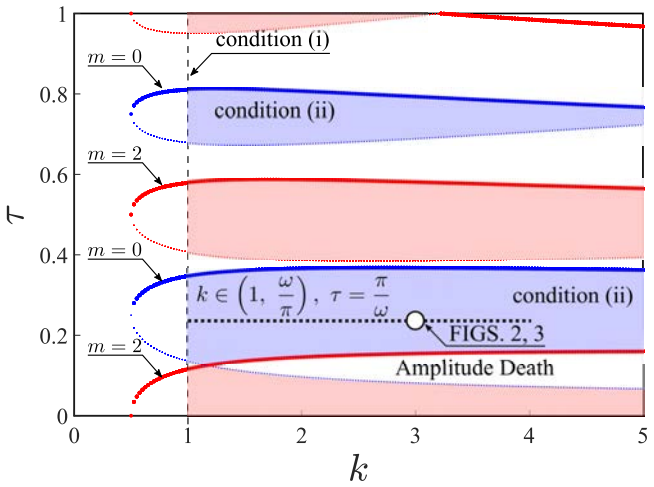

FIG. 4. Boundary curves for the existence of in-phase (i.e., $m = 0$) and antiphase (i.e., $m = 2$) synchronization and regions satisfying condition (ii) in (k, τ) parameter space.

Next, condition (iii) is discussed. To investigate the stability of the antiphase synchronization, Eqs. (6) and (7) are linearized around the state described by Eq. (8) with $m = 2$, as

$$\dot{\mathbf{x}}(t) = (\boldsymbol{I}_4 \otimes \boldsymbol{A})\mathbf{x}(t) + (\boldsymbol{C}_\mathrm{A} \otimes \boldsymbol{B})\mathbf{x}(t-\tau), \quad (12)$$

where

$$\mathbf{x}(t) := [\Delta r_1(t)\ \Delta\theta_1(t)\ \cdots\ \Delta r_4(t)\ \Delta\theta_4(t)]^T \in \mathbb{R}^8$$

$$\Delta r_j(t) := r_j(t) - \hat{r}, \ \ \Delta\theta_j(t) := \theta_j(t) - \hat{\theta}_j^{(2)}(t),$$

$$\boldsymbol{A} := \begin{bmatrix} -3\hat{r}^2 + 1 - k & k\hat{r}\sin\Omega\tau \\ -\frac{k}{\hat{r}}\sin\Omega\tau & k\cos\Omega\tau \end{bmatrix},$$

$$\boldsymbol{B} := \begin{bmatrix} -\frac{k}{2}\cos\Omega\tau & -\frac{k}{2}\hat{r}\sin\Omega\tau \\ \frac{k}{2\hat{r}}\sin\Omega\tau & -\frac{k}{2}\cos\Omega\tau \end{bmatrix}.$$

The diagonal transformation matrix $\boldsymbol{T}$: $\boldsymbol{T}^{-1}\boldsymbol{C}_\mathrm{A}\boldsymbol{T} = \mathrm{diag}(2, 0, 0, -2)$ allows the linearized system (12) to be simplified as follows:

$$\boldsymbol{z}_l = \boldsymbol{A}\boldsymbol{z}_l + \rho_l\boldsymbol{B}\boldsymbol{z}_l(t-\tau), \quad (l = 1, \ldots, 4),$$

where $\mathbf{x} = (\boldsymbol{T} \otimes \boldsymbol{I}_2)[\boldsymbol{z}_1^T \ \cdots \ \boldsymbol{z}_4^T]^T$. Here, $\rho_1 = 2$, $\rho_{2,3} = 0$, and $\rho_4 = -2$ are the eigenvalues of $\boldsymbol{C}_\mathrm{A}$. From this, the

[3] It should be noted that these curves are equivalent to the stability boundaries for the equilibrium point $Z_{1,\ldots,4} = 0$ of the oscillator networks described by Eqs. (1) and (2) with $\boldsymbol{C}_\mathrm{A}$.

characteristic function of the linear system in Eq. (12) is given by

$$f(s) := \prod_{l=1}^{4} g(\rho_l, s),$$

where

$$g(\rho_l, s) := \det[s\boldsymbol{I}_2 - \boldsymbol{A} - \rho_l e^{-s\tau}\boldsymbol{B}]. \tag{13}$$

Note that $f(s) = 0$ has one zero root $s = 0$, as $g(\rho_1, 0) = 0$ always holds; this zero root corresponds to the synchronization manifold. The antiphase synchronization state [Eq. (8)] with $m = 2$ is stable if and only if all the roots of $f(s) = 0$ except the zero root have negative real parts.

The above results are now summarized. Conditions (i), (ii), and (iii) hold if k and τ are selected such that the following three conditions are satisfied: (i) $k > 1$; (ii) k and τ are within the blue regions in Fig. 4 [i.e., Eqs. (10) and (11) hold]; (iii) all the roots of $f(s) = 0$ except the zero root have negative real parts. It should be noted that such a design procedure requires some complicated computations. Thus, we show that if $\omega > \pi$, the following simple procedure for determining k and τ can be used:

$$k \in \left(1, \frac{\omega}{\pi}\right), \quad \tau = \frac{\pi}{\omega}. \tag{14}$$

The horizontal dotted line in Fig. 4 represents the set of (k, τ) given by Eq. (14). The following demonstrates that k and τ in Eq. (14) satisfy conditions (i), (ii), and (iii). Condition (i) is obviously satisfied. For condition (ii), the existence of the antiphase ($m = 2$) and in-phase ($m = 0$) synchronization states are considered. For $m = 2$, there exists only the antiphase synchronization state with $\Omega = \omega$ and $\hat{r} = 1$. For $m = 0$, there exists only $\Omega = \omega$ satisfying Eq. (9b), and it also satisfies Eq. (11). As a result, the antiphase synchronization with $\Omega = \omega$ exists, and the in-phase synchronization does not exist. For condition (iii), the functions in Eq. (13) with the parameters given in Eq. (14), $\Omega = \omega$, and $\hat{r} = 1$, are simplified. The well-known analytical results for a one-dimensional linear delay system [34] then imply following: $g(\rho_1, s) = 0$ has a zero root, but the other roots have negative real parts; $g(\rho_{2,3}, s) = 0$ has the two roots $s = -k < 0$ and $s = -2 - k < 0$; and all the roots of $g(\rho_4, s) = 0$ have negative real parts. These analytical results indicate that the antiphase synchronization is stable. It should be noted that the unfilled circle on the dotted line in Fig. 4 represents the (k, τ) values used in Figs. 2 and 3.

In addition to determining k and τ, the switching rule that induces the suppression must be considered. It can be easily confirmed that the suppression mechanism described in the preceding subsection is valid for any switching order, i.e., $\boldsymbol{C}_A \leftrightarrows \boldsymbol{C}_B$, $\boldsymbol{C}_B \leftrightarrows \boldsymbol{C}_C$, and $\boldsymbol{C}_C \leftrightarrows \boldsymbol{C}_A$. This shows that the suppression can be induced not only by the periodic orderings given as examples in Fig. 2 but also by randomized orderings.

It would be interesting to examine how the number of oscillators and the types of topologies influence these analytical results. However, we focus here only on the four delay-coupled oscillators described by Eqs. (1) and (2) with the ring topology $\boldsymbol{C}(t) \in \{\boldsymbol{C}_A, \boldsymbol{C}_B, \boldsymbol{C}_C\}$, the simplest case for amplitude suppression, because the main purposes of the present paper are to report the occurrence of this suppression and to analytically and experimentally clarify its essential mechanism. Thus, the influence remains an issue to be investigated in future work.[4]

C. Numerical simulations

The influence of the connection parameters (k, τ) and the switching period T on the amplitude suppression was next numerically investigated. Figures 5(a)–5(d) show the average amplitude,

$$\delta := \frac{1}{4}\left\langle \sum_{j=1}^{4} |Z_j(t)| \right\rangle, \tag{15}$$

in the (k, τ) connection parameter space for the switching periods $T = 5$, 10, 20, and $T \to +\infty$ (i.e., invariant topology), respectively. It should be noted that the topology was changed in same manner as in Fig. 2(a) (i.e., $\boldsymbol{C}_A \leftrightarrows \boldsymbol{C}_B$). The four oscillators were isolated until $t = 10$, at which point they were coupled with the network topology $\boldsymbol{C}(t) = \boldsymbol{C}_A$. The topology then switched to $\boldsymbol{C}(t) = \boldsymbol{C}_B$ at $t = 10 + T$ and continued to alternate in this manner in time intervals of T. In Eq. (15), $\langle\cdot\rangle$ denotes averaging over $t \in [100, 400]$. The average amplitude δ was numerically estimated in 101×101 grids in (k, τ) space. The dark blue (yellow) regions in Fig. 5 represent areas of small (large) average amplitude. These figures show that the average amplitude depends on the switching period T. For $T = 5$ (10 times the natural period of 0.5), as shown in Fig. 5(a), the dark blue regions correspond to the blue regions in Fig. 4 except where $k \lesssim 1.5$. It can be seen from Figs. 5(b) ($T = 10$) and 5(c) ($T = 20$) that the dark blue regions shrink with increasing switching period T. For $T \to +\infty$, as shown in Fig. 5(d), the dark blue region remains only in the amplitude death region.

To clarify the dependence of the amplitude suppression on T, the time series data are shown in Figs. 6 and 7. The amplitudes are *not* suppressed in these cases, even though the coupling parameters satisfy conditions (i), (ii), and (iii). At $(k, \tau) = (1.50,\ 0.25)$ with $T = 5$ (i.e., the circle in Fig. 5(a)), the amplitudes are not suppressed, as shown in Fig. 6(a). Figure 6(b) shows an enlarged view at $t \in [17, 22]$ to clarify the reason for the failure of suppression. For $t \in [17, 20]$, the oscillators were coupled with $\boldsymbol{C}(t) \equiv \boldsymbol{C}_B$ and converged with antiphase synchronization [Eq. (3)]. As described earlier, suppression is the repetition of the following actions in order: antiphase synchronization, switching of the topology, amplitude decrease, switching to another antiphase synchronization state, and slow amplitude increase in this second antiphase synchronization state. However, Fig. 6(b) shows that the topology changes at $t = 20$, before the switch to the second antiphase synchronization [Eq. (5)]. Accordingly, the amplitudes did not converge to equilibrium points for $\boldsymbol{C}(t) \equiv \boldsymbol{C}_A$. However, Fig. 7 shows time series data at $(k, \tau) = (3.0,\ 0.25)$ with $T = 20$ [i.e., the circle in Fig. 5(c)]. At

[4]It should be noted that condition (ii) requires the formation of two clusters of antiphase synchronized oscillators; thus, condition (ii) is not valid for *odd* numbers of oscillators with a ring topology due to the impossibility of forming two such clusters.

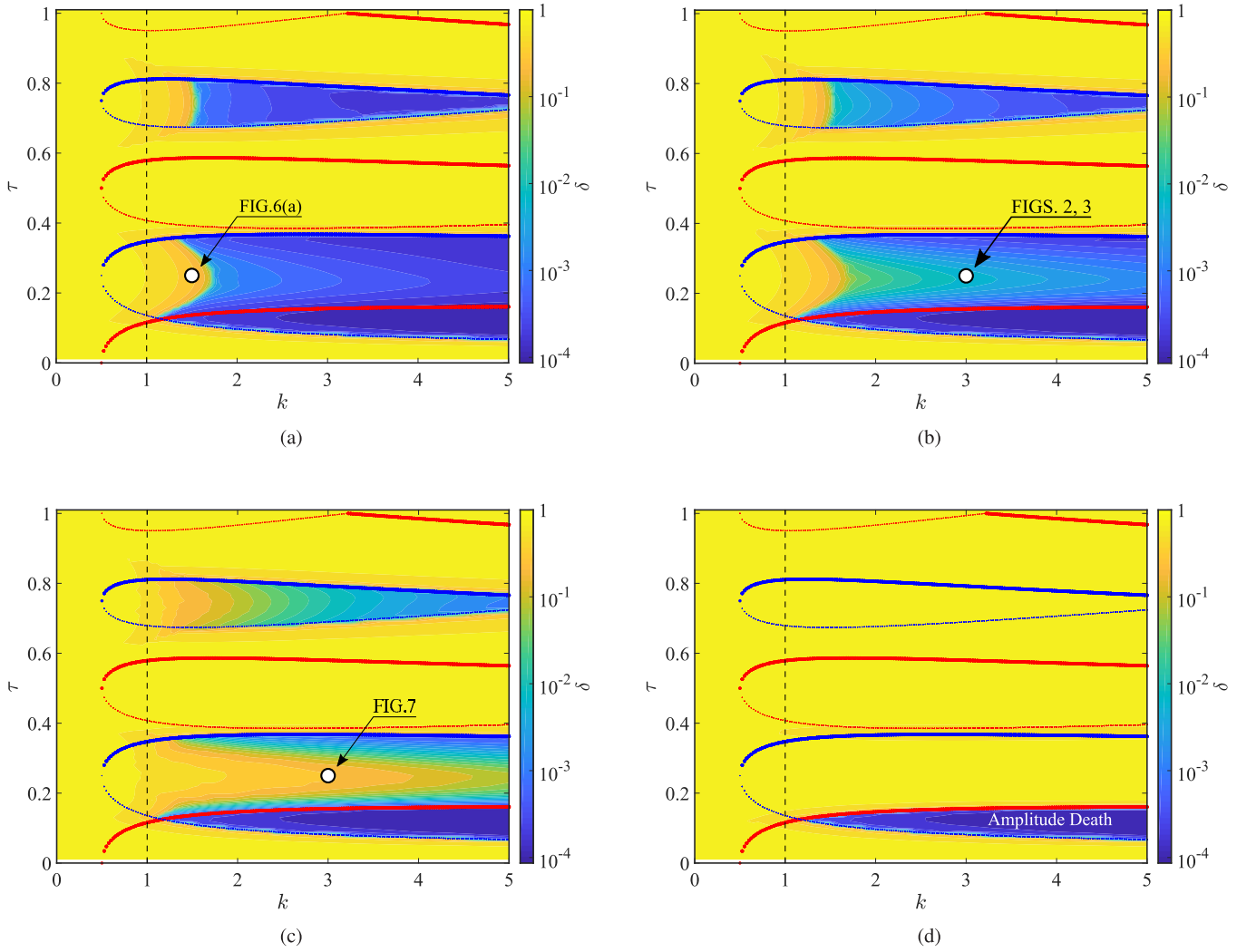

FIG. 5. Average amplitude δ in (k, τ) connection parameter space for switching periods (a) $T = 5$, (b) $T = 10$, (c) $T = 20$, and (d) $T \to +\infty$ (invariant topology).

$t = 30$, the amplitudes converged after the switching from $\boldsymbol{C}_{\mathrm{A}}$ to $\boldsymbol{C}_{\mathrm{B}}$; however, the amplitudes then fully grew before the next topology switch because the switching period was too long to maintain the suppressed state.

In addition, the relationship between the suppressed area in the parameter space (k, τ) and the switching period $T \in [0.5, 40]$ was numerically investigated in the same manner as in Fig. 5. Here, the switching period T was presumed to be longer than the natural period of the oscillator of $2\pi/\omega = 0.5$. An index was defined as

$$\beta[\%] := \frac{\text{Size of the suppressed area with } \delta \leqslant 10^{-3}}{\text{Size of space } (k, \tau) : k \in [0, 5] \text{ and } \tau \in [0.01, 1.01]} \times 100,$$

to evaluate the ratio of the size[5] of the suppressed area (i.e., blue regions in Fig. 5) to the size of (k, τ) parameter space. The index β is plotted against the switching period T in Fig. 8. The points at $T = 5$, 10, and 20 correspond to Figs. 5(a), 5(b) and 5(c), respectively. The inset in Fig. 8, which presents a detailed view of the data for $T \in [0.5, 5]$, shows that the index β is maximized at $T = 3$. For $T > 3$, the index β decreases as the switching period increases and then approaches the dashed line. The dashed line $\beta \approx 4.88\%$ denotes the ratio of the size of the amplitude death region to the size of (k, τ) space for the time-invariant network (i.e., $\boldsymbol{C}(t) \equiv \boldsymbol{C}_{\mathrm{A}}$, $\boldsymbol{C}_{\mathrm{B}}$, or $\boldsymbol{C}_{\mathrm{C}}$) shown in Fig. 5(d). As shown in Figs. 5(a), 5(b) and 5(c), the suppressed regions shrink with increasing switching period; however, these regions with $T = 5$, 10, and 20 commonly include the amplitude death region of the time-invariant network with $T \to +\infty$. In addition, we numerically estimated the index β as a function of T at the lower frequency $\omega = 2\pi$ and the higher frequency $\omega = 8\pi$: similar trends were observed.

The above discussion can be summarized as follows: the size of the suppressed area depends on the switching period T, and the slow-switching topology has the potential to enlarge the suppressed area relative to that of the time-invariant topology.

[5]Numerical simulations were conducted in 101 × 101 grids with $k \in [0, 5]$ and $\tau \in [0.01, 1.01]$. The size is given by the number of grid elements.

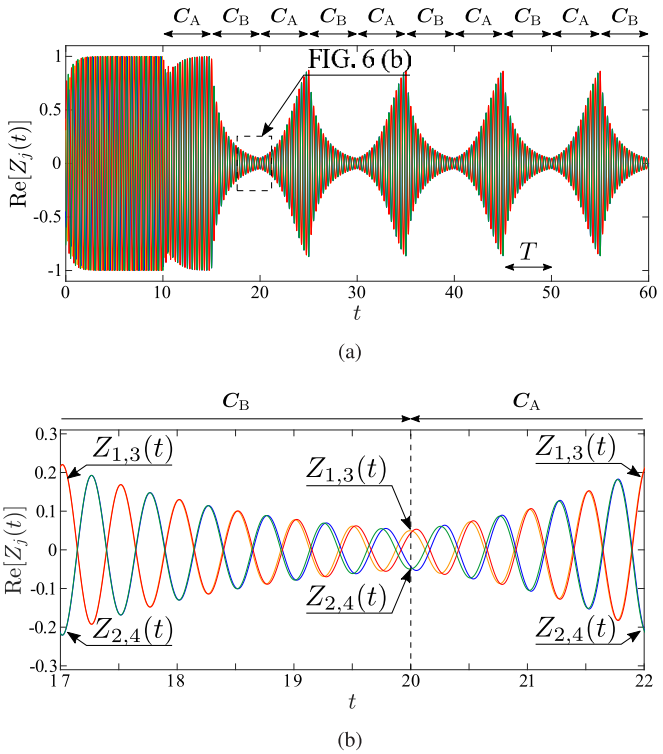

FIG. 6. Switching before suppression for (a) $t \in [0, 60]$ and (b) $t \in [17, 22]$: $k = 1.50$, $\tau = 0.25$, $T = 5.00$.

IV. CIRCUIT EXPERIMENTS

The preceding section analytically and numerically clarified the mechanism of amplitude suppression in Stuart–Landau oscillators, which are ideal oscillators near the Hopf bifurcation. The present section aims to experimentally demonstrate that amplitude suppression occurs even in *chaotic* oscillators.

Let us consider the double-scroll circuit $j \in \{1, \ldots, 4\}$ (see Fig. 9), which is a well-known chaotic oscillator [35] described by

$$C_a \frac{dv_a^{(j)}(t)}{dt} = \frac{1}{R_d}\{v_b^{(j)}(t) - v_b^{(j)}(t)\} - h(v_a^{(j)}),$$
$$C_b \frac{dv_b^{(j)}(t)}{dt} = \frac{1}{R_d}\{v_a^{(j)}(t) - v_b^{(j)}(t)\} + i_L^{(j)}(t) + i_u^{(j)}(t),$$
$$L \frac{di_L^{(j)}(t)}{dt} = -v_b^{(j)}(t),$$

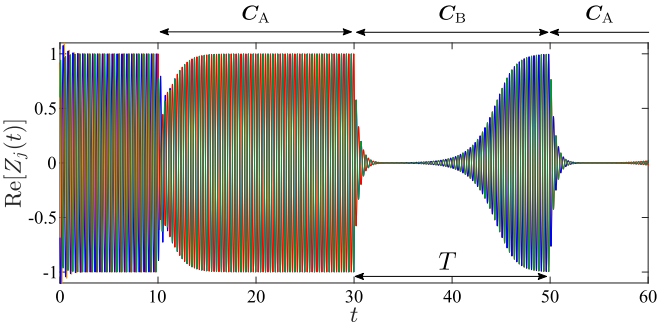

FIG. 7. Switching after amplitude growth: $k = 3.00$, $\tau = 0.25$, $T = 20.0$.

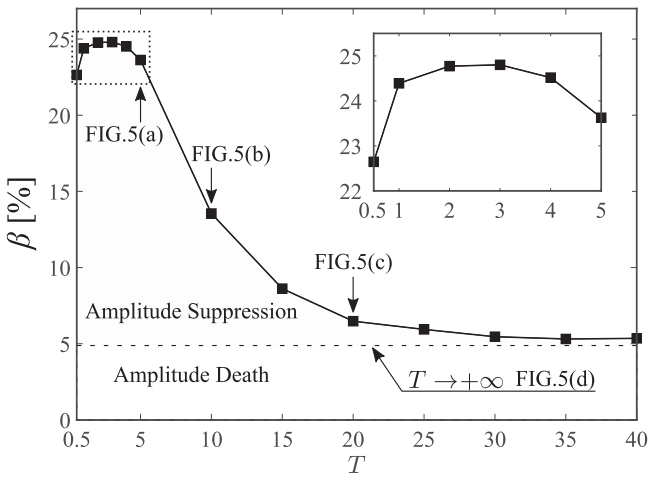

FIG. 8. Index β for suppression ratio plotted against switching period T with oscillator frequency $\omega = 4\pi$.

where $v_a^{(j)}(t)$ [V] and $v_b^{(j)}(t)$ [V] are the voltages applied to the respective capacitors C_a [F] and C_b [F], and R_d [Ω] is the circuit resistor. The currents $i_L^{(j)}(t)$ [A] and $h(v_a^{(j)})$ [A], respectively, flow through the inductor L [H] and the nonlinear resistor [36] given by

$$h(v) := m_0 v + \tfrac{1}{2}(m_1 - m_0)\{|v + B_p| - |v - B_p|\},$$

where m_0, m_1, and B_p are parameters. The coupling current from the other oscillators to the jth oscillator is described by

$$i_u^{(j)}(t) = \frac{R_d}{R_k} \sum_{l=1}^{4} c_{jl}(t)\{v_b^{(l)}(t - T_d) - v_b^{(j)}(t)\},$$

where T_d [s] is the delay time. The ratio $R_d/R_k > 0$ with the coupling resistor $R_k \in [180\,\Omega, 1800\,\Omega]$ represents the coupling strength.

The delay unit in Fig. 9 consists of level shift circuits, a PIC device (PIC18F2550), and an R–2R resistor ladder digital-to-analog converter [26,37]. The PIC device imports the voltage $v_b^{(j)}(t)$ with a sampling interval 25×10^{-6} s through the level shift circuit and the incorporated 10-bit analog-to-digital converter. The imported data $v_b^{(j)}(t)$ are stored in a first-in first-out queue on the PIC device for T_d [s]. The PIC device outputs the stored data as the delayed voltage $v_b^{(j)}(t - T_d)$ via the 8-bit digital-to-analog converter and the level shift circuit.

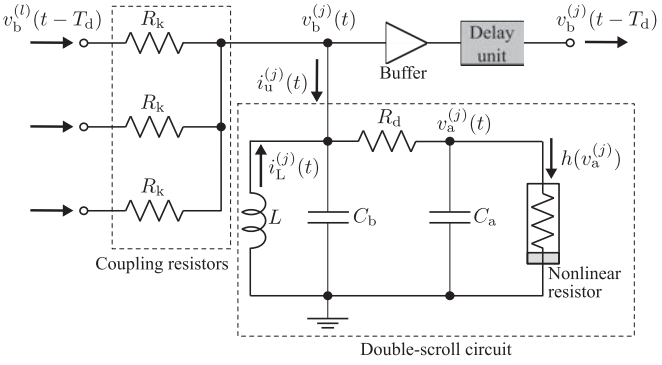

FIG. 9. Diagram of coupled double-scroll circuit.

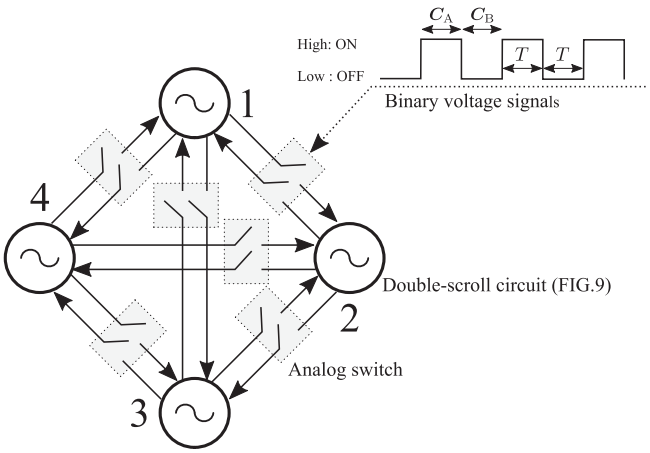

FIG. 10. Four double-scroll circuits with switching topologies.

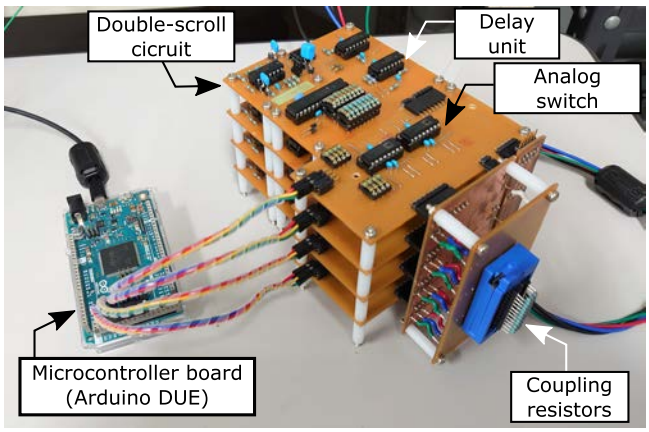

FIG. 11. Experimental setup of delay-coupled double-scroll circuits with time-varying topology.

The parameters for the double-scroll circuits are fixed at

$$C_a = 0.1\ \mu\text{F},\ C_b = 1.0\ \mu\text{F},$$
$$L = 180\ \text{mH}\ , B_p = 1.0\ \text{V},\ R_d = 1.8\ \text{k}\Omega,$$
$$m_0 = -0.4\ \text{mS},\ m_1 = -0.8\ \text{mS},$$

and the double-scroll chaotic attractor occurs in each circuit with a natural period[6] of $T_f \approx 3 \times 10^{-3}$ s. Here, the individual circuit has the following three unstable equilibrium points:

$$[v_a\ v_b\ i_L]^T = [0\ \ 0\ \ 0]^T,\ \left[\pm 2.57\quad 0\quad \mp 1.43 \times 10^{-3}\right]^T.$$

As illustrated in Fig. 10, the delay-coupled oscillator network consists of four double-scroll circuits (see Fig. 9) and analog switches (ADG452). These switches are controlled by the binary voltage signals corresponding to $c_{jl}(t) \in \{0, 1\}$, which is the (j, l)th element of the adjacency matrix $\boldsymbol{C}(t)$. A high (low) signal allows (does not allow) the delay voltage $v_b^{(l)}(t - T_d)$ to drive the coupling current $i_u^{(j)}(t)$ through the coupling resistor R_k. The binary voltage signals are controlled by a microcontroller board (Arduino Due). Figure 11 shows the experimental setup of the delay-coupled double-scroll circuits with a time-varying network; the four circuit board layers are connected by coupling resistors. Each board consists of a double-scroll circuit, a delay unit, and analog switches. The voltages $v_a(t)$ and $v_b(t)$ are imported into a personal computer (Windows 7 32bit, Intel Core i3-540, 2 GB RAM) through a 12-bit analog-to-digital input board (PCI-3153, Interface Corp.) at a sampling rate of 30 kHz and an input voltage range of ± 5 V.

The time series data for $v_b^{(j)}(t)$ $(j = 1, \ldots, 4)$ for $(R_d/R_k, T_d) = (4.85, 2.25 \times 10^{-3}\,\text{s})$ and $T = 150 \times 10^{-3}$ s are shown in Fig. 12. The four circuits were isolated until $t = 0.5$ s, and then coupled with $\boldsymbol{C}(t) = \boldsymbol{C}_A$. The network topology $\boldsymbol{C}(t) \in \{\boldsymbol{C}_A, \boldsymbol{C}_B\}$ alternated between the two possible states. As shown in Fig. 12(a), the amplitudes of all the circuits were suppressed around the equilibrium point $v_b = 0$ V.

[6]The natural period was estimated from the eigenvalue of the Jacobian matrix at the equilibrium points $[v_a\quad v_b\quad i_L]^T = [\pm 2.57\quad 0\quad \mp 1.43 \times 10^{-3}]^T$.

The occurrence of the amplitude suppression in double-scroll circuits was then confirmed. In Sec. III A, it was demonstrated that the essential mechanism of amplitude suppression in Stuart–Landau oscillators is the repetition of the following actions in order: antiphase synchronization, switching of the topology, amplitude decrease, switching to another antiphase synchronization state, and slow amplitude increase with this second antiphase synchronization state (see Fig. 3). Figures 12(b), 12(c) and 12(d) show enlarged views of the data at the first topology switch $\boldsymbol{C}_A \to \boldsymbol{C}_B$, the second switch $\boldsymbol{C}_B \to \boldsymbol{C}_A$, and the third switch $\boldsymbol{C}_A \to \boldsymbol{C}_B$, respectively. The enlarged view at $t \in [0.64\,\text{s}, 0.72\,\text{s}]$ [Fig. 12(b)] demonstrates that the voltage pairs $v_b^{(1,3)}(t)$ and $v_b^{(2,4)}(t)$ were synchronized until $t = 0.65$ s; however, the pairs $v_b^{(1,3)}(t)$ and $v_b^{(2,4)}(t)$ were not perfectly antiphase synchronized with each other. Just after $\boldsymbol{C}(t)$ switched from $\boldsymbol{C}_A$ to $\boldsymbol{C}_B$ at $t = 0.65$ s, the voltages $v_b^{(j)}(t)$ were suppressed and began to oscillate immediately because they were not completely antiphase synchronized. The voltages $v_b^{(j)}(t)$ were observed to increase with antiphase synchronization, as

$$v_b^{(1)}(t) \approx v_b^{(2)}(t) \approx -v_b^{(3)}(t) \approx -v_b^{(4)}(t). \tag{16}$$

The topology changed at $t = 0.80$ s [see Fig. 12(c)], and then all the voltages $v_b^{(j)}(t)$ converged to the equilibrium point $v_b = 0$ V. For $\boldsymbol{C}(t) = \boldsymbol{C}_A$, the voltages $v_b^{(j)}(t)$ strayed from the antiphase synchronization state described in Eq. (16) because of the noise, and then, as illustrated in Fig. 12(d), they switched to another antiphase synchronization state,

$$v_b^{(1)}(t) \approx -v_b^{(2)}(t) \approx v_b^{(3)}(t) \approx -v_b^{(4)}(t).$$

Furthermore, the voltages $v_b^{(j)}(t)$ were suppressed when the topology switched at $t = 0.95$ s. After the suppression, the voltages slowly increased. This observation demonstrates that amplitude suppression can occur not only in Stuart–Landau oscillators (i.e., ideal limit-cycle oscillators) but also in double-scroll circuits (i.e., chaotic oscillators) by the same mechanism.

Section III C showed the influence of the coupling parameters (k, τ) and the switching period T on amplitude suppression in Stuart–Landau oscillators (see Fig. 5). On

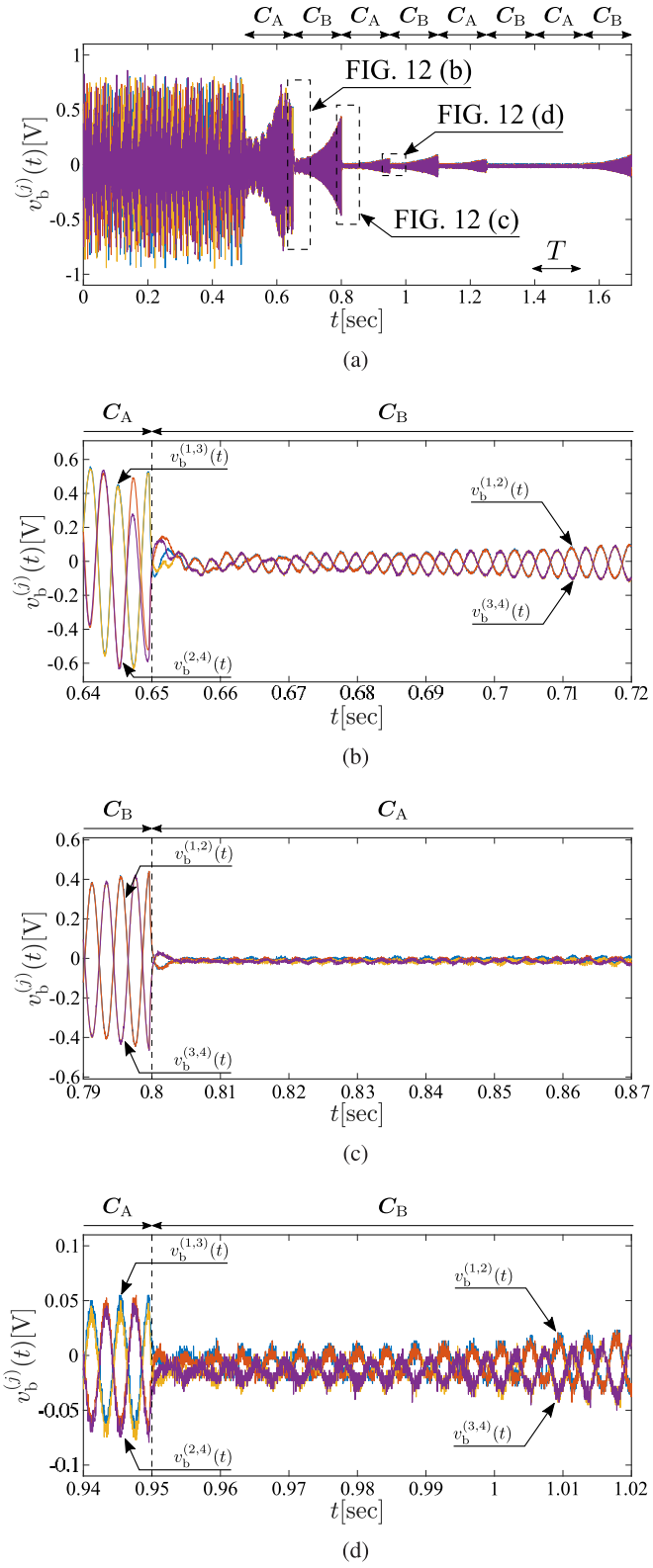

FIG. 12. Time-series data for $v_b^{(j)}(t)$ for $(R_d/R_k, T_d) = (4.85, 2.25 \times 10^{-3}\,\mathrm{s})$ and $T = 150 \times 10^{-3}$ s. (a) $t \in [0\,\mathrm{s}, 1.7\,\mathrm{s}]$, (b) $t \in [0.64\,\mathrm{s}, 0.72\,\mathrm{s}]$, (c) $t \in [0.79\,\mathrm{s}, 0.87\,\mathrm{s}]$, and (d) $t \in [0.94\,\mathrm{s}, 1.02\,\mathrm{s}]$.

this theoretical basis, the influence of the coupling parameters $(R_d/R_k, T_d)$ and switching period T [s] on amplitude suppression in double-scroll circuits was experimentally demonstrated. Figure 13 shows the experimental results in $(R_d/R_k, T_d)$ connection parameter space for the switching periods $T = 30 \times 10^{-3}$ s, 150×10^{-3} s, 300×10^{-3} s and $T \to +\infty$ (time-invariant topology), respectively. The plotted circles represent the average amplitude,

$$\delta := \frac{1}{4}\left\langle \sum_{j=1}^{4} |v_b^{(j)}(t)| \right\rangle,$$

where $\langle\cdot\rangle$ denotes the average over $t \in [1.2\,\mathrm{s}, 1.7\,\mathrm{s}]$. The blue (yellow) circles indicate a small (large) amplitude. Figures 13(a)–13(c) demonstrate that the blue circles (i.e., the suppressed region) depend on the switching period T [s]. It should be noted that the switching periods $T = 30 \times 10^{-3}$, 150×10^{-3}, and 300×10^{-3} s are much longer than the natural period of the double-scroll circuits, which is $T_f \approx 3 \times 10^{-3}$ s. Figure 13(d) shows the experimental results for a time-invariant network (i.e., $T \to +\infty$); amplitude death occurs in the region of the blue circles. It was observed that the time-varying networks have larger suppressed regions than the time-invariant network, which is consistent with Fig. 5. Figure 13 demonstrates that the suppressed regions shrink with increasing switching period and that these regions in the case of $T = 30 \times 10^{-3}$, 150×10^{-3}, and 300×10^{-3} s commonly include the amplitude death region of the time-invariant network. These experimental results are consistent with the numerical results presented in Sec. III C.

V. CONCLUSIONS

This paper presented an investigation of amplitude suppression in a delay-coupled oscillator network with a time-varying topology in which the topology changes at a rate much lower than the oscillator frequency. It was revealed that the mechanism behind the suppression is repetition of the following actions in order: antiphase synchronization, switching of the topology, amplitude decrease, switching to another antiphase synchronization state, and slow amplitude increase with the second antiphase synchronization state. The mechanism was verified numerically with the Stuart–Landau oscillator, and a procedure for determining the coupling parameters (k, τ) to induce the suppression was presented on the basis of the mechanism. The suppressed regions in (k, τ) connection parameter space depend on the switching period T. The time-varying networks were found to have a larger suppressed region than the time-invariant network. Furthermore, the amplitude suppression phenomenon was observed with double-scroll circuits. The experimental results demonstrate that amplitude suppression can occur not only in the Stuart–Landau oscillators but also in the double-scroll chaotic circuits by the same mechanism.

ACKNOWLEDGMENT

The present study was supported in part by JSPS KAKENHI (Grant No. 18H03306).

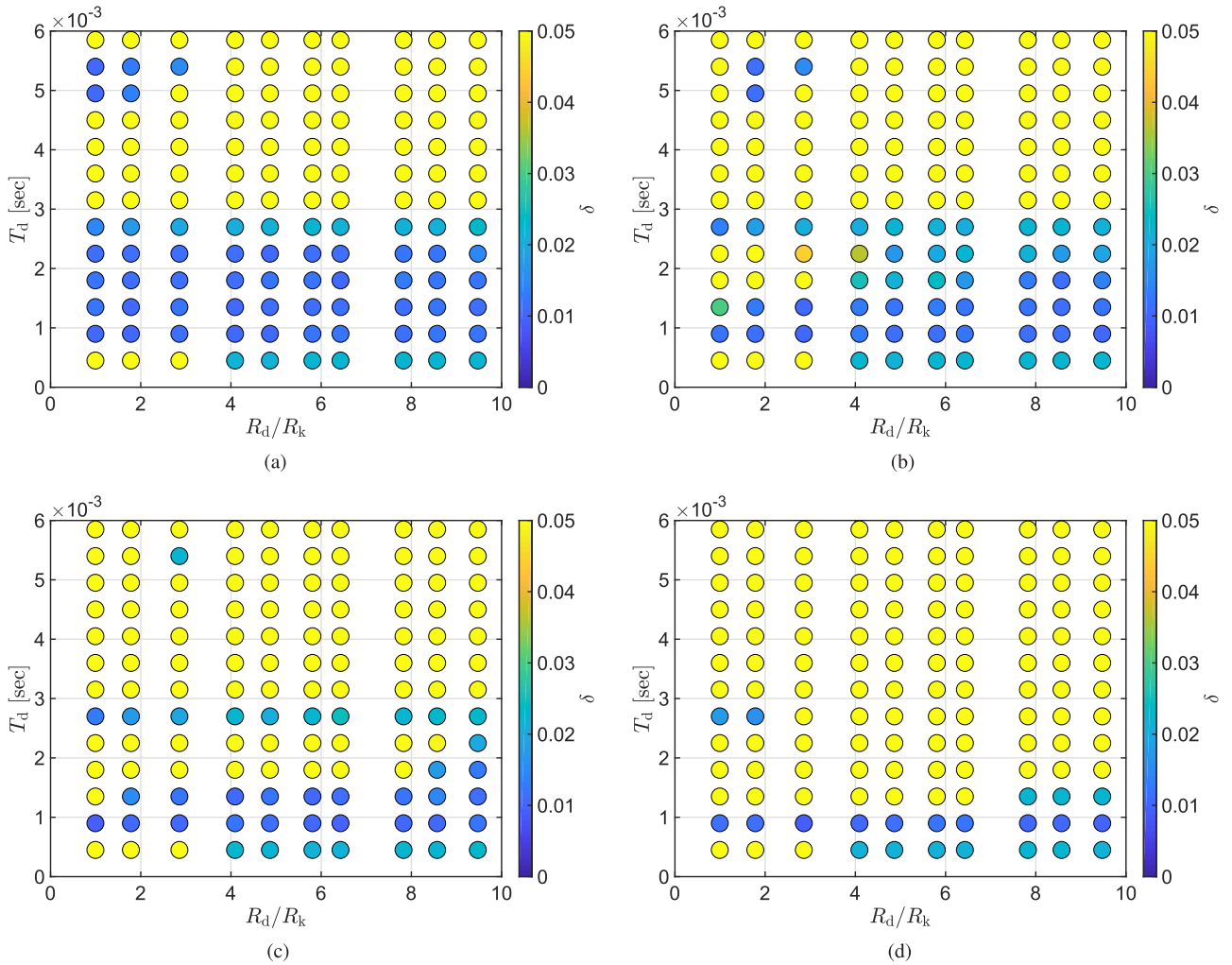

FIG. 13. Average amplitude δ in $(R_d/R_k, T_d)$ connection parameter space for switching periods (a) $T = 30 \times 10^{-3}$ s, (b) $T = 150 \times 10^{-3}$ s, (c) $T = 300 \times 10^{-3}$ s, and (d) $T \to +\infty$ (invariant topology).

[1] G. Saxena, A. Prasad, and R. Ramaswamy, Phys. Rep. **521**, 205 (2012).
[2] A. Koseska, E. Volkov, and J. Kurths, Phys. Rep. **531**, 173 (2013).
[3] S. Huddy and J. Skufca, IEEE Trans. Power Elect. **28**, 247 (2013).
[4] T. Biwa, S. Tozuka, and T. Yazaki, Phys. Rev. Appl. **3**, 034006 (2015).
[5] H. Hyodo and T. Biwa, Phys. Rev. E **98**, 052223 (2018).
[6] K. Bar-Eli, Physica D **14**, 242 (1985).
[7] R. Mirollo and S. Strogatz, J. Stat. Phys. **60**, 245 (1990).
[8] K. Gupta and G. Ambika, Chaos **29**, 033119 (2019).
[9] D. V. Ramana Reddy, A. Sen, and G. L. Johnston, Phys. Rev. Lett. **80**, 5109 (1998).
[10] S. Strogatz, Nature **394**, 316 (1998).
[11] K. Konishi and N. Hara, Phys. Rev. E **83**, 036204 (2011).
[12] R. Karnatak, R. Ramaswamy, and A. Prasad, Phys. Rev. E **76**, 035201(R) (2007).
[13] D. Ghosh and T. Banerjee, Phys. Rev. E **90**, 062908 (2014).
[14] T. Banerjee and D. Ghosh, Phys. Rev. E **89**, 052912 (2014).
[15] F. Atay, Phys. Rev. Lett. **91**, 094101 (2003).
[16] W. Michiels and H. Nijmeijer, Chaos **19**, 033110 (2009).
[17] M. Mehta and A. Sen, Phys. Lett. A **355**, 202 (2006).
[18] W. Zou, C. Yao, and M. Zhan, Phys. Rev. E **82**, 056203 (2010).
[19] Y. Sugitani, K. Konishi, L.B. Le, and N. Hara, Chaos **24**, 043105 (2014).
[20] Y. Guo and B. Niu, Nonlinearity **28**, 1841 (2015).
[21] S.R. Huddy and J. Sun, Phys. Rev. E **93**, 052209 (2016).
[22] W. Zou, D. Senthilkumar, R. Nagao, I. Kiss, Y. Tang, A. Koseska, J. Duan, and J. Kurths, Nat. Commun. **6**, 7709 (2015).
[23] Y. Sugitani and K. Konishi, Phys. Rev. E **96**, 042216 (2017).
[24] H. Teki, K. Konishi, and N. Hara, Phys. Rev. E **95**, 062220 (2017).
[25] Y. Sugitani, K. Konishi, and N. Hara, *Nonlinear Dynamics of Electronic Systems* (Springer, Cham, 2014), pp. 219–226.
[26] S. Masamura, T. Iwamoto, Y. Sugitani, K. Konishi, and N. Hara, Nonlin. Dyn. **99**, 3155 (2020).
[27] T. Iwamoto, Y. Sugitani, S. Masamura, K. Konishi, and N. Hara, in *Proceedings of the International Symposium on Nonlinear Theory and its Applications* (IEICE, Tokyo, Japan, 2018), pp. 487–490.

[28] S. Chaurasia, A. Choudhary, M.D. Shrimali, and S. Sinha, Chaos, Solitons Fractals **118**, 249 (2019).
[29] C. Pereti and D. Fanelli, Chaos, Solitons Fractals **133**, 109587 (2020).
[30] R. Dodla, A. Sen, and G.L. Johnston, Phys. Rev. E **69**, 056217 (2004).
[31] P. Perlikowski, S. Yanchuk, O.V. Popovych, and P.A. Tass, Phys. Rev. E **82**, 036208 (2010).
[32] C.-U. Choe, T. Dahms, P. Hövel, and E. Schöll, Phys. Rev. E **81**, 025205(R) (2010).
[33] K. Blaha, J. Lehnert, A. Keane, T. Dahms, P. Hövel, E. Schöll, and J. L. Hudson, Phys. Rev. E **88**, 062915 (2013).
[34] J. Hale and S. Lunel, *Introduction to Functional Differential Equations* (Springer, New York, 1993).
[35] T. Matsumoto, L. Chua, and M. Komuro, IEEE Trans. Circuits Sys. **32**, 797 (1985).
[36] M. Kennedy, Frequenz **46**, 66 (1992).
[37] Y. Sugitani, K. Konishi, and N. Hara, Nonlin. Dyn. **70**, 2227 (2012).